Parallel-Computing Wavelet-Based FDTD Method for Modeling Nanoscale Optical Resonator

Jiang Xiyan(蒋锡燕), *Wang Jin*(王瑾)*, *Lu Yunqing*(陆云清), *Xu Ji*(许吉)

School of Optoelectronic Engineering, Nanjing University of Posts and Telecommunications, Nanjing, 210023, P. R. China

(Received 16 May 2013; revised 17 December 2013; accepted 20 December 2013)

Abstract: An efficient wavelet-based finite-difference time-domain (FDTD) method is implemented for analyzing nanoscale optical devices, especially optical resonator. Because of its highly linear numerical dispersion properties the high-spatial-order FDTD achieves significant reduction in the number of cells, i. e. used memory, while analyzing a high-index dielectric ring resonator working as an add/drop multiplexer. The main novelty is that the wavelet-based FDTD model is extended in a parallel computation environment to solve physical problems with large dimensions. To demonstrate the efficiency of the parallelized FDTD model, a mirrored cavity is analyzed. The analysis shows that the proposed model reduces computation time and memory cost, and the parallel computation result matches the theoretical model.

Key words: integrated optics; electromagnetic field analysis; finite difference time domain (FDTD); wavelet; parallel computation

CLC number: O441.4 **Document code**: A **Article ID**: 1005-1120(2014)03-0260-09

1 Introduction

The optical devices in modern optical communication systems tend to be miniaturized, while many light-processing functions are integrated within a small chip area. Normally, these optical devices are high-index structures, e. g. silicon optical devices, which have a large refractive index variation within the circuit layout. As a result, the physical dimensions of these optical devices are comparable with the wavelength of the optical signals. Therefore, full-vector solutions are desired in order to obtain an accurate solution.

The finite-difference time-domain (FDTD) method[1-3], which solves time-dependent Maxwell's curl equations numerically, has been proved to be a highly efficient technique for numerous applications in electromagnetics. Since the method makes very few assumptions and includes the total field in its simulation, both the reflected field and the forward propagation field are part of the solution.

Despite of the simplicity of the FDTD method, this technique suffers serious limitations in case that substantial computer resource is required to solve electromagnetic problems with medium or large computational dimensions. Especially, analysis of optical waveguide with a 3D FDTD method is often computationally too large. This is because the FDTD method requires a discretization of a twentieth of the target wavelength for accurate computations. This situation becomes even worse in a longer waveguide, which requires a finer discretization due to the cumulative numerical dispersion error of the FDTD method. However, the available memory hinders such a 3D analysis in most optical waveguides.

Recently, it has been shown in many re-

Foundation items: Supported by the Scientific Research Foundation of Nanjing University of Posts and Telecommunications (NY212008, NY213116); the National Science Foundation of Jiangsu Province (BK20131383).

* **Corresponding author**: Wang Jin, Professor, E-mail: jinwang@njupt.edu.cn.

search fields that the wavelets theory is a very efficient algorithm to solve differential equations numerically[4]. In Refs. [5—7], a high-order finite-difference scheme has been developed, which is based on Daubechies compactly supported orthogonal wavelets[8] and Deslauriers-Dubuc interpolating functions[9] as biorthogonal wavelet bases. This modified time-domain scheme shows highly linear dispersion characteristics and brings significant reductions of the memory usage. Thus, other continuing works have been preceded to improve the efficiency of this wavelet collocation method, e. g. by introducing structured non-orthogonal discretization grids into such methods[10] or by adapting the computational grid at each time step[11]. However, because a finer resolution is required for investigating and designing nanoscale optical devices, e. g. silicon or plasmonic optical devices, this wavelet-based FDTD method still suffers a huge memory demand.

The new contribution of this work is that the wavelet-based FDTD method from Refs. [5—7] has been extended on a parallel-computational IBM cluster to further improve the computation efficiency. Before parallelizing the wavelet-based FDTD method, this method is implemented, i. e. programmed on a stand-alone computer, to verify the highly linear dispersion characteristics of this method. In Section 2, it shows that this method requires less memory, while a same accuracy is kept as that by using the standard FDTD method. In Section 3, the parallelization of the wavelet-based FDTD method is realized on the IBM cluster. To calculate an optical device, the wavelet-based FDTD method uses several processors which operate in parallel on different parts of the calculation space and exchange information on the boundaries. To handle the parallel computation and the data exchange, the message passing interface (MPI) software package is used to create a program easily portable to the cluster. The simulation results show not only a memory-saving but also a time-saving in calculation by using the wavelet-based FDTD method and parallel-computing in the MPI environment.

2 Electromagnetic Field Analysis with Wavelet-Based FDTD

The wavelet-based FDTD method is used to calculate the propagation of an electromagnetic field. For optical devices are of few hundred nanometer scale, it is still valid to deploy a classical description of the electromagnetic properties of matter, i. e. neglect quantum mechanical phenomena. These properties of electromagnetic fields are governed by the Maxwell equations. The FDTD method solves Maxwell's curl equations directly. It means that the update equations are derived directly from the curl equations and yield solutions for the electric field E and the magnetic field H at certain points in time and space[1]. Naturally, space and time must be discretized to enable a computational treatment. Following Ref. [1], a space grid point is denoted by integers i, j and k, i. e. $(i,j,k) = (i\Delta x, j\Delta y, k\Delta z)$, Δx, Δy and Δz are the space increments. The time step is Δt and the nth time step is $n\Delta t$. Thus, a function of space and time can be denoted as $F(i\Delta x, j\Delta y, k\Delta z, n\Delta t) = F(i,j,k,n)$. For almost all numerical techniques, the proper choice of the sampling width plays a crucial role in the performance of the algorithm. For FDTD algorithms the sampling space is determined by the highest near-field spatial frequency of interest. Typically, a sampling rate in space is needed to be below $\lambda/20$. The choice of the sampling rate in time is restricted by the sampling in space to ensure stability[2].

The wavelet-based FDTD method is to solve the time-dependent Maxwell's curl equations by using the wavelet-collocation formulation. The wavelet-collocation formulation developed in Refs. [5—7] uses Deslauriers-Dubuc (DD) interpolating functions[9] as the basis functions, which form the compactly supported biorthogonal wavelet bases. The associated basis functions are denoted as DD2, DD4 and DD10 for respective interpolating orders[6]. Because of the interpolation property of this family of wavelets, their expan-

sion coefficients can represent field values directly. A short review of the formulation[5-7] is given in Appendix A.

The numerical formulation given in Appendix A is implemented, i. e. programmed to analyze electromagnetic fields in optical devices. The optical device analyzed first is a 3D optical ring resonator, as shown in Fig. 1. The different areas are for the actual calculation region, the perfectly matched layers (PML)[12], the perfectly conducting layers (PCL), respectively. Note that this optical device has the same dimensions as those in Ref. [13], because we want to establish a wavelet-FDTD model firstly and prove it. The structure parameters of this ring resonator are given briefly as follows. The waveguide layer has a height of 0.405 μm, while the bottom substrate layer and the upper air layer are 1.5 times higher than the waveguide. The refractive indices of the waveguide and the substrate are 3.03 and 1.67, respectively. The radius and width of the ring are 2.25 μm and 0.5 μm, respectively, while the straight waveguide is 0.55 μm wide. The gaps between the straight and the ring waveguides are chosen to be 0.2 μm. In total, the size of the problem is 8.3 μm in length, 7.1 μm in width and 1.62 μm in height. An absorbing boundary condition (ABC) with five anisotropic perfectly matched layers (APML) is applied to terminate the computation region. This promises a less than −50 dB reflection as depicted in Ref. [14]. The field-launching and monitoring ports are also depicted in Fig. 1. They are located in the straight waveguides and have the same height and width as those of the straight waveguide.

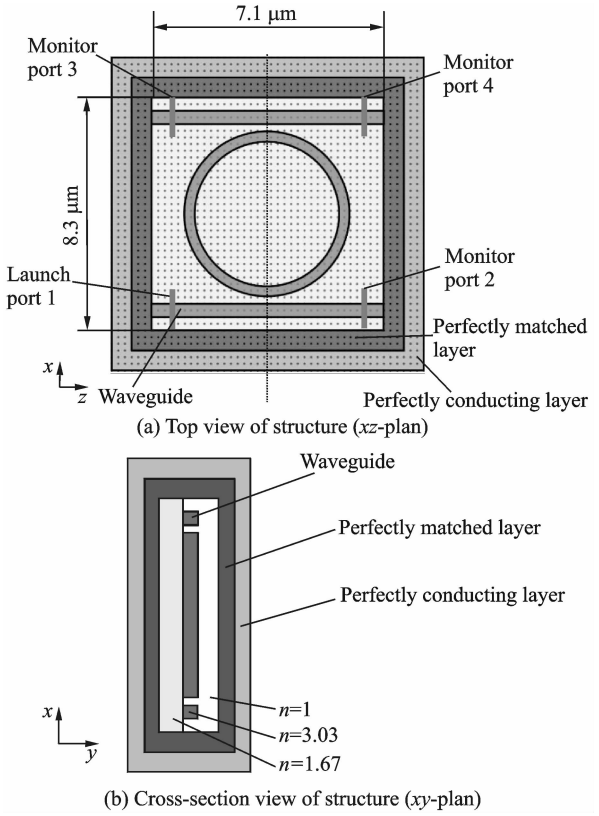

Fig. 1 3D optical ring resonator[13]

The evolution of electromagnetic fields in this structure is simulated. First of all, the steady-state propagation mode for the initial excitation is needed. Such a mode is calculated in a Fabry-Perot straight waveguide, each end of which is truncated by a perfect electric wall. The waveguide structure of this resonator has the same cross section as the straight one in Fig. 1 (b), while the waveguide length is chosen to ensure a half-sine longitudinal distribution at the resonance frequency within the frequency range of interest, from 130 THz to 200 THz. Into this waveguide resonator, a field with a Gaussian transversal distribution and a half-sine longitudinal distribution is launched, see Fig. 2(a). The dominant propagation mode is then obtained as the field evolves in the time domain, Fig. 2(b). This propagation mode is indeed the eigen-mode of this resonator structure. The obtained eigen-mode field is successively used as an excitation template for simulating the pulse propagation.

After the excitation field is introduced to the launch port 1, seen in Fig. 1, the evolution of electromagnetic fields in this structure is simulated. The evolution time duration is set to be 600 fs, the targeted center frequency to be 150 THz and the polarization component to be E_y resulting in a TM polarization. Calculated by using the DD4 basis function with a discretization $\Delta=0.05$ μm (DD4, 0.05) for all three space directions, the E_y-field evolutions on the y-normal plane at the half-height of the waveguide are shown in Fig. 3, where the observation time is 10 fs and 140 fs after the excitation signal is

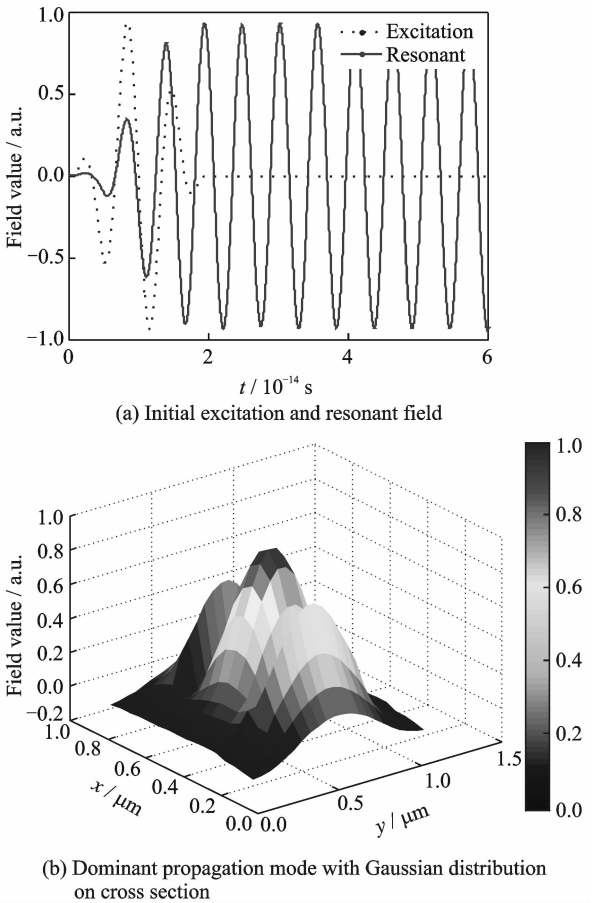

Fig. 2 Steady-state initial excitation and resonant signal

launched into structure.

The transmission S-parameter (S21) and the coupling S-parameter (S31), which describe how much the excitation field at the launch port 1 is coupled to the monitor port 2 and 3, are extracted by means of a discrete Fourier transform of the FDTD time series data of each port and depicted in Fig. 4. To check the accuracy of the model, the transmission S-parameter (S21) and the coupling S-parameter (S31) are compared between the DD4 and the standard FDTD by choosing different Deslauriers-Dubuc interpolating basis functions, as explained in Appendix A. The choice of the DD4 basis functions is based on the demonstration[5-7] that using the standard FDTD basis functions with a space discretization (0.025 μm) still gives a higher numerical error than using the DD4 basis functions with a doubled space discretization (0.05 μm).

The feasibility and accuracy of our model are proved by the results shown in Fig. 4(a), which

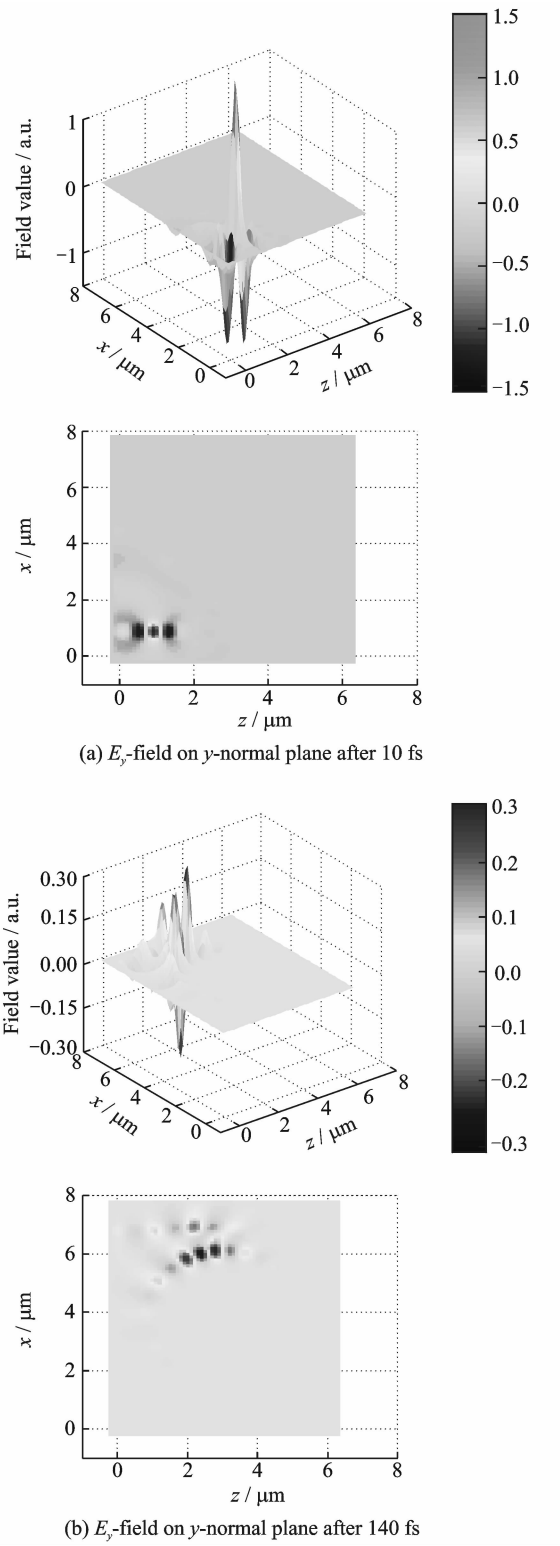

Fig. 3 Field evolution of TM-polarized E_y component on y-normal plane at half-height of waveguide

are very similar to those results shown in Ref. [13]. It can be seen in the DD4 time evolution, Fig. 4(b), that the resonant frequency at the port 3 is 154.24 THz, which is found with a reasonable frequency resolution of 0.032 THz for the dis-

crete Fourier transform. This finest frequency resolution is restricted by the frequency error in this scheme, which is 0.016% around 200 THz, yielding 0.032 THz. In the case of the standard FDTD time evolution, the resonant frequency is 153.92 THz using a frequency resolution of 0.36 THz, which is restricted by the frequency error in this scheme. These results are very similar to the results in Ref. [13], where the calculated resonant frequency is about 153.75 THz. The next resonant frequency calculated in our model is 159.64 THz, which is also matching those from the most recent reference[15], where a three-dimensional full vectorial finite-element method was used to simulate the same structure in Fig. 1. This comparison shows that our model works fine.

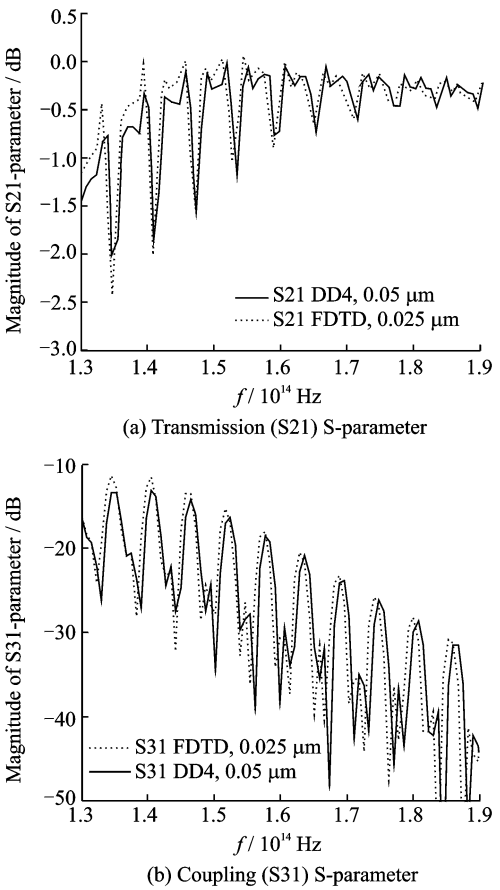

Fig. 4 Transmission (S21) S-parameter and coupling (S31)S-parameter of ring resonator filter shown in Fig. 1 for TM-polarized field

The required computational resources needed for the above two computation methods are compared and listed in Table 1. These computations are performed on a windows-PC with an AMD Athlon(TM) processor (a single core clock of 2.3 GHz) and a 3 GB memory. The numbers in Table 1 emphasize the stated major drawback of all FDTD-based computational methods. Even a rather small structure with a coarse discretization mesh needs a fair amount of CPU time and memory. E. g., by choosing the DD4 method with a space discretization of 0.05 μm, the computation takes about 28.9 h and occupies 122 MB memory. This problem gets even worse if a finer resolution is required, e. g. for the DD4 method with a discretization of 0.025 μm in Table 1. In this case, not only the number of the grid points increases by a factor of eight, but also the number of the time steps also increases. Therefore, the required memory increases in a cubic manner, and the CPU-time increases with fourth order for a finer gridding. It is evident that a larger problem space is not solvable in a reasonable time for stand-alone computers using these FDTD-based methods.

Table 1 Required computational resources used for analyzing structure shown in Fig. 1

Scheme	DD4	FDTD	DD4
Discretization Δ/μm	0.05	0.025	0.025
Nbr. of cell	324×68×264	628×116×508	648×136×528
Nbr. of time step	31 027	12 665	37 232
Memory used/MB	122.0	600.5	600.5
CPU time/h	28.9	31.5	99.0

3 Parallel-Computing Wavelet-Based FDTD Technique

The extensive memory and time consumption of FDTD algorithms limit their scope of application. These two problems can both be tackled by employing a parallel working algorithm[16]. This means implementing the wavelet-based FDTD technique on a parallel-computing machine. The used parallel machine locates at the computer center of the Karlsruhe Institute of Technology, where an IBM RS/6000 SP- SMP is equipped.

The SMP machine consists of 256 processors. Each processor has a clock rate of 375 MHz and a memory of 1 GB. The software solution for establishing the communication in the distributed memory systems is the message passing interface (MPI) standard[17].

The basic idea of the parallelization is computing different parts of a task simultaneously. That means a splitting of the calculation region in a number of subregions, which can be treated separately from each other and can therefore be processed in a parallel way. In the parallelization, the shape and size of the partitions of the calculation region are crucial parameters influencing the efficiency of the algorithm. As we use a Cartesian grid and all of our calculation regions are cuboids, cubical partitions are a straightforward solution. Moreover, most of the integrated electro-optical devices of interest are "flat", i. e. at least one spatial extension is considerably smaller than the other two. Thus, we implements a two-dimensional distribution of the subregions, seen in Fig. 5.

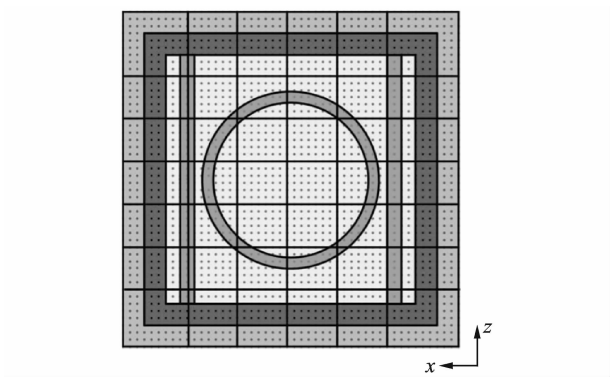

Fig. 5 Splitting of calculation area in Fig. 1 into different subregions

Fig. 5 depicts how the calculation region of a ring-resonator structure is split into 42 subregions. It can be seen that these subregions are differently sized. This is due to the consideration that the neighboring grid-points of one subregion have to be updated using other grid-points in their own grid circumference. As this goes on, an ever bigger part of the calculation region has to be taken into account. This situation can be explained via Fig. 6.

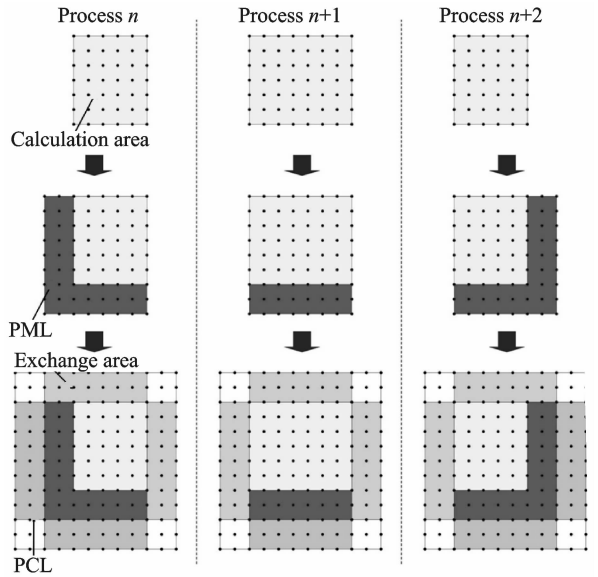

Fig. 6 Creating of calculation space of three processors

Fig. 6 shows how to create the calculation space for three processors, while different areas are for the actual calculation region, the PML, the PCL and the exchange area in subregions, respectively. By considering the extra exchange area, all subregions have a same total calculation region.

The parallelized wavelet-based FDTD method needs to be verified. The best way to verify the proper function of the numerical algorithm is to consider a structure with analytically accessible solutions of the governing physical equations. One of these simple structures is a metallic box filled with a homogeneous medium (e. g. air). It works as a resonator and the field energy should go into a set of modes which represent standing waves inside the box. The resonant frequencies that characterize the standing waves depend on the size of the box and are

$$f_{k,l,m} = \frac{2}{c_0}\sqrt{\frac{k^2}{L_x} + \frac{l^2}{L_y} + \frac{m^2}{L_z}} \tag{1}$$

where L_x, L_y and L_z denote the spatial extensions of the box in x, y and z directions respectively. The integer values k, l and m stand for mode's order; at least two of them must be nonzero.

To demonstrate the efficiency of the parallelization, a box with dimension of 1.026 5 μm × 0.923 9 μm × 1.385 7 μm is chosen, and the pro-

gram is ran with 1, 4, 9, 12, and 16 processors. It should be noted that the number of allocated processors is up to 16. This is the maximum number allowed by the administration, because other users are sharing the parallel computer. To compare the simulation results with the theoretical values, the field data at different grid points inside the box is collected and the power spectrum is calculated, e. g. for the E_x-component (f_{011}) shown in Fig. 7. The values of the obtained resonant frequencies are summarized in Table 2. It can be seen that these results match the theoretical values. There is also a small deviation between theoretical and simulated values. One reason for the small deviation lies in that the size of the calculation region differs slightly for different numbers of processors. That is because we have to use an integer number of cells in each direction.

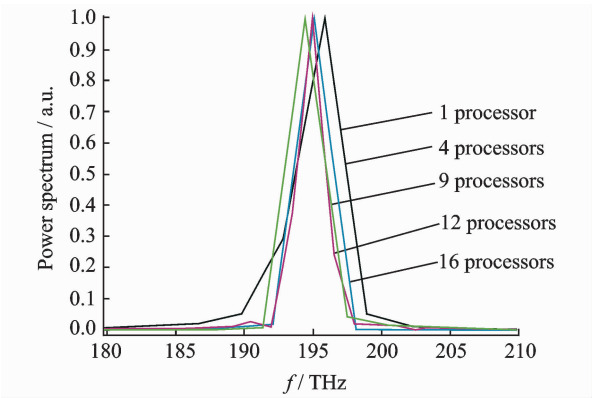

Fig. 7 Resonant frequencies of E_x-component (f_{011}) for different processor numbers allocated in parallel computation

Table 2 Resonant frequencies in rectangular cavity when the number of processors varies from 1 to 16

Frequency mode	f_{011}/THz	f_{101}/THz	f_{110}/THz
Theoretical value	195.13	181.85	218.44
1 processor	194.52	179.08	219.22
4 processors	194.52	179.08	219.22
9 processors	195.97	180.66	217.4
12 processors	195.05	179.93	217.73
16 processors	195.19	179.94	219.59

The way to demonstrate the efficiency of the parallelization is the speed-up achieved with an increasing number of processors. As the program is run with 1, 4, 9, 12, and 16 processors, the runtimes is recorded and compared in Fig. 8. It can be seen that the gain of time-saving by applying the parallel computation in this problem is already a factor of 10.3 for an allocation of 16 processors, and the occupied memory in each processor is also much decreased in proportion with the increase of the total processor number. This result proves that this parallelized program is promising to solve physical problems with large dimensions.

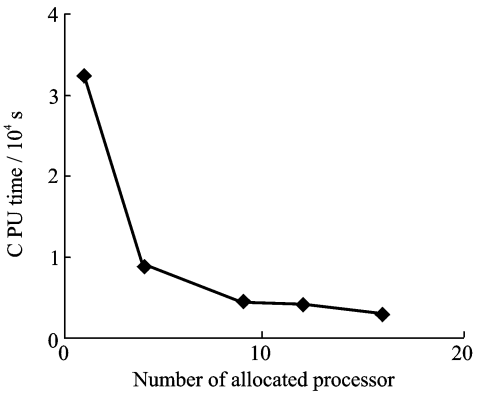

Fig. 8 Comparison of CPU time in one processor for different processor-allocations

4 Conclusions

A high-order wavelet-based FDTD scheme has been implemented to analyze optical devices in a 3D case. The high-order schemes have a better linear numerical dispersion than that of the standard FDTD method, thus allowing coarser space discretization. This leads to a significant reduction of the required memory. Beyond that, to gain a reduction in the computation time, the wavelet-based FDTD method is parallelized in the MPI environment. A computation result for a metallic box by implementing the parallelized model shows a factor of 10.3 for an allocation of 16 processors. The parallel-computing model is promising to analyze more complicated optical devices with large dimensions.

The most important criterion for the calculation efficiency in the parallel computation environment is how good the load sharing works. If

there is a strong mismatch between the workload of the different processors, the run time of the slowest machine limits the speed. Therefore, it is worth having a similar load sharing between different processors.

Besides, the efficiency of this model can be further improved by implementing a multi-grid technique in the FDTD algorithm. Via a multi-grid technique, the staircase numerical error can be mitigated as other thoughts, e. g. a finite element method[15].

Acknowledgement

The author would like to thank Professor W Freude in Karlsruhe Institute of Technology for helpful discussion.

Appendix A: Wavelet-based FDTD method

The wavelet-based FDTD method developed in Refs. [5-7] uses the Deslauriers-Dubuc (DD) interpolating functions[9] as the basis functions, which form the compactly supported biorthogonal wavelet bases. The DD interpolating function $\phi(x)$ is, indeed, an autocorrelation function of the Daubechies scaling function $\varphi_0(x)$[8]

$$\phi(x) = \int_{-\infty}^{\infty} \varphi_0(u)\varphi_0(u-x)\mathrm{d}u \tag{A. 1}$$

The shifted and contracted scaling function gives the associated wavelet function $\psi(x)$

$$\psi(x) = \phi(2x-1) \tag{A. 2}$$

The scaling function $\phi(x)$ satisfies the so-called dilation relation[8]

$$\phi(x) = \sum_{k=-\infty}^{+\infty} h_k^{\mathrm{DD}} \phi(2x-k) \tag{A. 3}$$

where h_k^{DD} is the filter coefficients[8], and $k=1,2,\cdots,p-1$. The coefficients h_k^{DD} for $p=2,4,10$ can be found in Ref. [7]. The associated basis functions are denoted as DD2, DD4 and DD10 for respective p. For $p=1$, namely DD1, it turns out to be the standard FDTD.

As given in Ref. [5], the time-dependent electromagnetic field is modeled through the wavelet-Galerkin procedure. The Galerkin's procedure proceeds as follows[18]:

(1) The expanded field variables are substituted into Maxwell's equations.

(2) The equations are then tested with the dual basis functions, where "test" means the inner product between the expanded field variables and the dual basis[5-7].

(3) At last, the biorthogonality condition $\langle \phi_m, \tilde{\phi}_q \rangle = \delta_{mq}$, for m or $q=0,1,\cdots,p-1$, is applied.

The scaling functions $\phi(x)$ in Eq. (A. 1) in space and the Haar scaling functions[19] $h(t)$ in time are used to expand the electromagnetic fields. E. g., the component F_x (either E_x or H_x) is expanded as

$$F_x(x,y,z,t) = \sum_{i,j,k,n=-\infty}^{+\infty} F^x_{i+1/2,j,k,n+1/2}\, \phi_{i+1/2}(x)\phi_j(y)\phi_k(z)h_{n+1/2}(t) \tag{A. 4}$$

where $h_n(t) = h\left(\frac{t}{\Delta t} - n + \frac{1}{2}\right)$. Note that the subscript x of F_x in the left side of Eq. (A. 4) is moved to the superscript position in the right side of Eq. (A. 4).

By applying the biorthogonality condition, the time evolution equations similar to the multi-resolution time-domain (MRTD) method[19] are obtained. In a medium with a permittivity ε, a permeability μ, and a conductivity σ in presence of a current density J, the components E_x and H_x evolve as[7]

$$E^x_{i+1/2,j,k,n+1/2} = \frac{2\varepsilon - \sigma\Delta t}{2\varepsilon + \sigma\Delta t} E^x_{i+1/2,j,k,n-1/2} + \frac{2\Delta t}{2\varepsilon + \sigma\Delta t} \times \left[\sum_{l=-L_s}^{L_s-1} a(l)\left(\frac{H^z_{i+1/2,j+l+1/2,k,n}}{\Delta y} - \frac{H^y_{i+1/2,j,k+l+1/2,n}}{\Delta z}\right) - J^x_{i,j,k,n}\right] \tag{A. 5}$$

$$H^x_{i,j+1/2,k+1/2,n+1} = H^x_{i,j+1/2,k+1/2,n} - \frac{\Delta t}{\mu} \sum_{l=-L_s}^{L_s-1} a(l) \times \left(\frac{E^z_{i,j+l+1,k+1/2,n+1/2}}{\Delta y} - \frac{E^y_{i,j+1/2,k+l+1,n+1/2}}{\Delta z}\right) \tag{A. 6}$$

The sum in Eqs. (A. 5, A. 6) is taken according to the number of the connection coefficients $a(l)$; L_s gives the support of the basis functions, i. e., the number of coefficients per side. The values of the connection coefficients $a(l)$ can be found in Ref. [7], in which the equations for other E and H components can also be found.

The evolution of the electromagnetic fields should maintain the numerical accuracy and computational stability. These requirements depend on the choice of the space grid and the time increment. Naturally, the change of electromagnetic field over the chosen space grid size should not be very big. Thus, for a computational stability, it is necessary to satisfy a relation between the space grid and the time increment Δt. The stability criterion implemented in this work is[7]

$$\Delta t \leqslant \left[c_0 \left(\sum_{l=0}^{L_s-1} |a(l)|\right) \sqrt{\left(\frac{1}{\Delta x}\right)^2 + \left(\frac{1}{\Delta y}\right)^2 + \left(\frac{1}{\Delta z}\right)^2}\right]^{-1} \tag{A. 7}$$

where c_0 is the speed of light.

It should be noticed that in most optical waveguide problems the problem space must be truncated, and a proper ABC must be applied to these truncation planes. The ABC requires that the waves arriving at the region boundaries should be absorbed without generating significant reflections. Thus, following the detailed description in Ref. [7], an APML is implemented in this work.

References:

[1] Yee K S. Numerical solution of initial boundary value

problems involving Maxwell′s equation in isotropic media[J]. IEEE Trans Antennas Propagation, 1966, 14(3):302-307.

[2] Taflove A. Advances in computational electrodynamics: The finite-difference time-domain method[M]. Boston: Artech House, 1998.

[3] Chen Y, Liu Y, Chen B, et al. A cylindrical higher-order FDTD algorithm with PML and quasi-PML [J]. IEEE Transactions on Antennas and Propagation, 2013,61(9):4695-4704.

[4] Glswami J C, Chan A K. Fundamentals of wavelets: Theory, algorithms and applications [M]. New York: Wiley Interscience, 1999.

[5] Fujii M, Hoefer W J R. Dispersion of time domain wavelet-Galerkin method based on Daubechies′ compactly supported scaling functions with three and four vanishing moments [J]. IEEE Microwave Guided Wave Lett, 2000,10(4):125-127.

[6] Fujii M, Hoeffer W J R. Application of biorthogonal interpolating wavelets to the Galerkin scheme of time dependent Maxwell′s equations[J]. IEEE Microwave and Wireless Components Lett, 2001,11(1):22-24.

[7] Fujii M, Hoeffer W J R. A wavelet formulation of finite difference method full vector analysis of optical waveguide junctions[J]. IEEE J Quantum Electronics, 2001,37(8):1015-1029.

[8] Daubechies I. Orthonormal bases of compactly supported wavelets[J]. Comm Pure and Appl Math, 1988,41(7):909-996.

[9] Deslauriers G, Dubuc S. Symmetric iterative interpolation processes[M]. New York: Constr Approx, 1989:49-68.

[10] Armenta R B, Sarris C D. A general procedure for introducing structured nonorthogonal discretization grids into high-order finite-difference time-domain methods[J]. IEEE Trans Microw Theory Tech, 2010,58(7):1818-1829.

[11] Li H. Numerical simulation of a micro-ring resonator with adaptive wavelet collocation method[D]. Germany: Karlsruhe Institute of Technology, 2011.

[12] Berenger J P. A perfectly matched layer for the absorption of electromagnetic waves [J]. J Comput Phys, 1994,114(2):185-200.

[13] Fujii M, Freude W, Russer P. Efficient high-spatial-order FDTD analysis of 3D optical ring resonator filters[C]//Proc 19th Annual Rev Progress in Appl Comput Electromagnetics. Monterey, CA: IEEE Computer Society Press, 2003:739-744.

[14] Gedney S D. An anisotropic perfectly matched layer absorbing medium for the truncation of FDTD lattices [J]. IEEE Trans Antennas Propagat, 1996, 44(12): 1630-1639.

[15] Milanovic B, Radjenovic B, Radmilovic-Radjenovic M. Three dimensional finite element modeling of optical microring resonators[J]. Physica Scripta, 2012 (T149):014026.

[16] Trobec R, Vajtersic M, Zinterhof P. Parallel computing: Numerics, applications, and trends[M]. London: Springer-Verlag, 2009.

[17] Message Passing Interface Forum. MPI: A message-passing interface standard[EB/OL]. (1995-06-12) [2012-03-11]. http://www.netlib.org/mpi/mpi-report.ps.

[18] Wang J J H. Generalized moment methods in electromagnetics: Formulation and computer solution of integral equations[M]. New York: Wiley, 1991.

[19] Krumpholz M, Katehi L. MRTD: New time-domain schemes based on multiresolution analysis[J]. IEEE Trans Microw Theory Tech, 1996, MTT-44(4): 555-571.

(Executive editor: Xu Chengting)